Demodulation scheme for fiber Bragg grating sensors based on active control of the spectral response of a wavelength division multiplexer

Francisco M. Araújo, Luís A. Ferreira, José L. Santos, and Faramarz Farahi

We present a closed-loop technique for measuring wavelength shifts associated with fiber Bragg gratings by using a fused biconical wavelength division multiplexer (WDM). The spectral response of the WDM is actively tuned by stretching of the coupling region to maintain a fixed coupling ratio at the reflected Bragg wavelength. The closed-loop operation allows sensitivities usually associated with a highly selective WDM to be obtained without compromising the measurement range. A simple theoretical model is presented together with experimental results for temperature and strain measurements.

OCIS codes: 060.1810, 060.2340, 060.2370.

1. Introduction

In the past few years, fiber Bragg grating (FBG) temperature and strain sensors and their application in smart structures and composite materials have been the subject of considerable research effort.[1–5] The small Bragg wavelength shifts associated with this class of sensor often require expensive and complex demodulation schemes. To widen the range of possible applications, it is desirable to develop simple techniques that utilize robust and low-cost components. Several filtering techniques have been demonstrated that fulfill these requirements, such as those based on bulk filters,[6] fiber edge filters,[7–9] edge optical source spectra,[10] edge fiber grating spectra,[11] edge detector response,[12] tunable fiber filters,[13] tunable acousto-optic filters,[14] and receiving FBG.[15] Among these, one of the most elegant methods is based on using a commercially available wavelength division multiplexer (WDM).[7] Although the measurement range obtained is large, the sensitivity is limited by the small slope of the WDM transfer function. For overcoming this problem, dedicated highly overcoupled couplers have been used.[8] The increased slope yields higher sensitivity but reduces the linear measurement range. As in other filtering techniques, active tuning would be an obvious solution to maintain high sensitivities with increased operating range. Mechanically polished couplers are well recognized by their excellent tunability properties through control of the effective interaction length.[16,17] However, these involve complex fabrication processes that result in very sensitive but expensive devices. The fusion biconical taper technique offers an attractive alternative for lossless and low-cost fabrication.[18] Although these devices are usually packaged to present a high-stability spectral response, one can adjust their coupling ratio by using techniques such as bend, twist, or axial strain induced on the tapered region and variations of the external refractive index.[19–24]

In this paper we show that it is possible to obtain a large measurement range by active control of a fused biconical WDM and take advantage of its high sensitivity. By stretching the coupling region, we demonstrate that the spectral characteristic of a WDM can be effectively tuned over ranges exceeding 15 nm without additional loss. These characteristics are useful for analysis of the optical signal returned from a fiber Bragg grating sensor, as we discuss in the following sections.

F. M. Araújo, L. A. Ferreira, and J. L. Santos (jlsantos@goe.fc.up.pt) are with the Unidade de Tecnologia Optoelectrónica, Instituto de Engenharia de Sistemas e Computadores, Porto, Rua do Campo Alegre, 687, 4150 Porto, Portugal. J. L. Santos is also with the Departamento de Física da Universidade do Porto, Rua do Campo Alegre, 687, 4150 Porto, Portugal. F. Farahi is with the Department of Physics, University of North Carolina at Charlotte, Charlotte, North Carolina 28223.

Received 9 June 1998; revised manuscript received 11 August 1998.

0003-6935/98/347940-07$15.00/0

2. Theory

The power at the output ports of a fused biconical tapered coupler, P_1 and P_2, can be written as

$$P_1 = P_0 \sin^2(CL), \tag{1}$$

$$P_2 = P_0 \cos^2(CL), \tag{2}$$

where P_0 is the power reaching the WDM, L is the interaction length, and C, the coupling constant, is given by[25]

$$C = \frac{3\pi\lambda}{32 n_2 a^2} \frac{1}{(1 + 1/V)^2}, \tag{3}$$

where λ is the operating wavelength, n_2 is the silica refractive index, a is the diameter of the biconical taper waist, and $V = 2\pi a/\lambda(n_2^2 - 1)^{1/2}$ is the normalized frequency. In this simplified model, the effects of polarization have been neglected, it is assumed that only two modes exist in the coupling region, and the cross section is considered constant over the entire coupling length. Using the above equations, we can derive an expression for the WDM period ($\Delta\lambda$):

$$\Delta\lambda = \frac{32 n_2 a^2}{3L} \frac{(1 + 1/V)^3}{(1 - 1/V)}. \tag{4}$$

During the coupler fabrication process a fixed length L_H of fiber is uniformly heated and stretched. In this condition the biconical taper diameter is expected to vary with taper elongation L_T as[26]

$$a(L_T) = a_0 \exp(-L_T/2L_H), \tag{5}$$

where a_0 is the initial fiber diameter.

The set of Eqs. (1) and (2) suggests that it is possible to modify the spectral response of a WDM by changing either the length of the coupling region L or the coupling constant C. For a limited range of wavelengths the coupling constant cannot be easily changed to obtain a desired spectral response after the fabrication process is completed. However, this change can be accomplished by proper control of the coupling length. From Eqs. (1) and (2), for equal power to be obtained at both output ports, the operating wavelength λ_{3dB} must satisfy

$$\lambda_{3dB} \approx \frac{8 n_2 a^2}{3L} (1 + 1/V)^2, \tag{6}$$

where V is approximately constant for a limited wavelength range. Because the required values of elongation are always small compared with the total coupling length L, a linear relation exists between $\Delta\lambda_{3dB}$ and ΔL:

$$\Delta\lambda_{3dB} \approx -\frac{8 n_2 a^2}{3L^2} (1 + 1/V)^2 \Delta L. \tag{7}$$

In obtaining Eq. (7) it was assumed that the imposed elongation is restricted to the coupling region. This in practice is a valid approximation since the cross section of the coupling region is very small when compared with the transition section of the taper ($a^2/a_0^2 < 10^{-3}$).[26] Also, small strain-induced refractive-index variations were neglected. As an example, Fig. 1 shows the tuning characteristics obtained for three WDM's with the same period $\Delta\lambda = 10$ nm, but with different fabrication parameters. As predicted by the model, Fig. 1 illustrates that for a fixed WDM period better wavelength tunability may be obtained when the length of fiber heated during the fabrication process is shorter, corresponding to higher values of the ratio a/L. It is also important to examine the tunability for different WDM periods. Since large values of a/L lead to a longer WDM period, better tunability is expected for devices with long periods. Figure 2 shows this dependency for three different values of L_H.

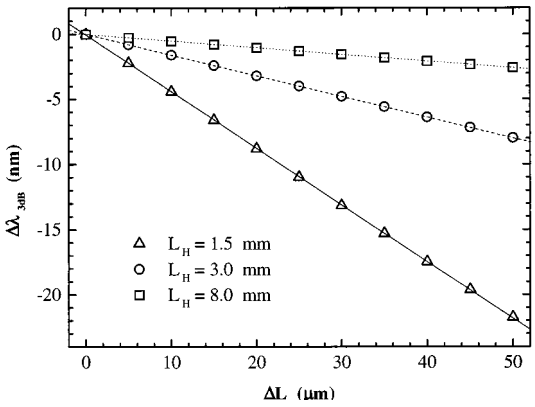

Fig. 1. Tuning characteristics for three WDM's with 10-nm periods and different fabrication parameters.

We now provide an analysis that describes the application of the WDM as a wavelength discriminator for FBG sensors. Consider the experimental setup in Fig. 3. The optical power at the output ports can be written as

$$P_1 \approx P_0\left(\frac{2\pi}{\Delta\lambda} V' \lambda_B - \frac{\pi}{4} + \frac{1}{2}\right), \tag{8}$$

$$P_2 \approx P_0\left(-\frac{2\pi}{\Delta\lambda} V' \lambda_B + \frac{\pi}{4} + \frac{1}{2}\right), \tag{9}$$

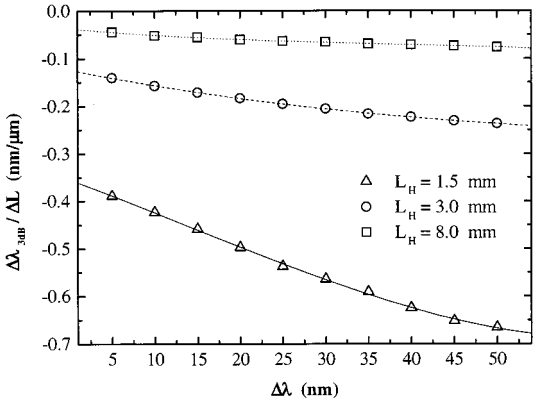

Fig. 2. Tunability as a function of the WDM period for three different fabrication parameters.

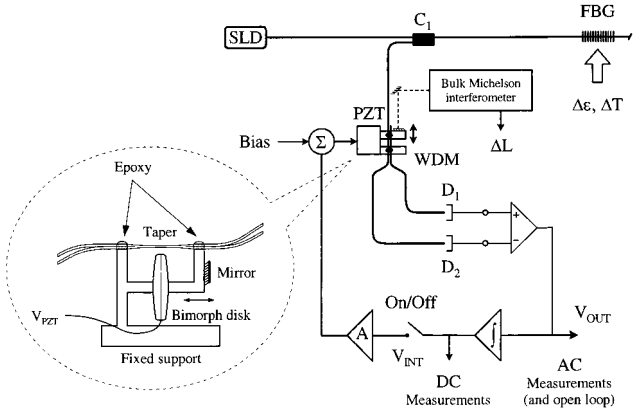

Fig. 3. Experimental setup. Inset: detail of the WDM stretching mount.

where λ_B is the Bragg wavelength, V' is given by $V' = (V + 1)/(V - 1)$, and P_0 is the power reaching the WDM after being reflected from the FBG. Approximations (8) and (9) are valid only for small Bragg wavelength shifts around the 3-dB point and for a grating spectral width much smaller than the WDM period. The signal after the differential amplifier is then given by

$$V_{\text{dif}} = KP_0 \frac{2\pi}{\Delta\lambda} V'(\lambda_B - \lambda_{3\text{dB}}), \tag{10}$$

where K is the gain of the detectors and $\lambda_{3\text{dB}}$ is the Bragg wavelength that sets $P_1 = P_2$. Equation (10) clearly shows that the system sensitivity to shift in the Bragg wavelength increases in proportion to the optical power reaching the WDM, and it is inversely proportional to the WDM period. However, minimizing the WDM period seriously restricts the linear measurement range. In other words, while it is advantageous to increase the slope by using a highly selective WDM, the maximum wavelength shift that can be detected in the linear region around the 3-dB point becomes smaller. To overcome this limitation, we propose a closed-loop approach (Fig. 3). By locking the 3-dB point of the WDM to the reflected Bragg wavelength, we can obtain high sensitivity without compromising the measurement range. The elongation applied to the WDM in closed-loop operation can be written as

$$\Delta L = \Delta L_{\text{Bias}} + K_{\text{PZT}} \frac{A}{\tau_C} KP_0 \frac{2\pi}{\Delta\lambda} V' \int (\lambda_B - \lambda_{3\text{dB}})\mathrm{d}t. \tag{11}$$

In Eq. (11), ΔL_{Bias} is the initial elongation necessary to ensure proper selection of the 3-dB point, K_{PZT} is the voltage to displacement conversion factor for the PZT used to stretch the WDM, A is the amplifier voltage gain, and τ_C is the integrator time constant. Equation (11) indicates that ΔL can be used to measure directly the Bragg wavelength shifts associated with strain or temperature variations applied to the FBG.

The sensitivity of the proposed demodulation scheme is basically determined by the system's noise level and the slope of the WDM spectral response. The most important noise source in the system is caused by the electronic circuitry, which is not related with power reaching detectors or WDM characteristics. That is, for a given optical source power the wavelength selectivity of the WDM dictates the minimum Bragg wavelength shift that can be measured. It is important to emphasize at this point that there are always practical limitations in the selection of WDM with a minimum period. The first limitation arises during the fabrication process, because a highly selective WDM requires long pulling that leads to excess power loss, incomplete mode conversion, and a fragile device. On the other hand, as can be seen in Fig. 2, higher wavelength selectivity corresponds to a reduced tuning capability of the WDM. This decrease in the tuning capability puts practical constraints on the WDM stretching when used in a closed loop. For this problem to be minimized, a short heating length should be used during the WDM fabrication process, as indicated by the data in Fig. 2. However, for a given selectivity, the minimum taper length is limited by mode-coupling loss, as described by the condition for adiabaticy.[27] Therefore the optimum period for the WDM used to analyze shift in the wavelength of light reflected from a FBG is determined by the power loss that can be accepted and the required maximum tunability range.

3. Experimental Results and Discussion

To demonstrate the effectiveness of the proposed demodulation scheme, we implemented the setup shown in Fig. 3. Light from a pigtailed superluminescent diode ($\lambda_0 = 1280$ nm, $\Delta\lambda_S = 20$ nm) was used to illuminate the FBG. The grating was written by the phase mask technique in hydrogen-loaded telecommunication fiber ($\lambda_B = 1282$ nm, $\delta\lambda = 0.2$ nm). To measure the Bragg wavelength shifts, we fabricated a WDM by using the fused biconical taper method. The fibers were uniformly heated over a length of 3.0 mm and elongated by 25.5 mm. The WDM period obtained was measured with an optical spectrum analyzer as $\Delta\lambda = 9.8$ nm. Using the experimental values of L_H, L_T, and $\Delta\lambda$ in Eqs. (4) and (5), we can estimate the value for the WDM waist, $a = 2.1$ μm, and for the coupling length, $L = 9.6$ mm. A typical WDM response is shown in Fig. 4.

Signals from detectors ($K = 500$ mV/μW) were used as inputs to a differential amplifier with unity gain. The typical optical power reaching detectors was ≈10 nW. Through the integrator a compensation signal is then generated when the power reaching detectors D_1 and D_2 is not balanced. This signal, after being amplified and added to a bias signal, is applied to the piezoelectric transducer (PZT) used to stretch the WDM structure. As mentioned in Section 2, the PZT bias is used to select an initial 3-dB point suitable to lock the Bragg wavelength. This situation is illustrated in Fig. 5. The WDM tunability can be estimated as $\Delta\lambda_{3\text{dB}}/\Delta L = -0.16$ nm/μm by

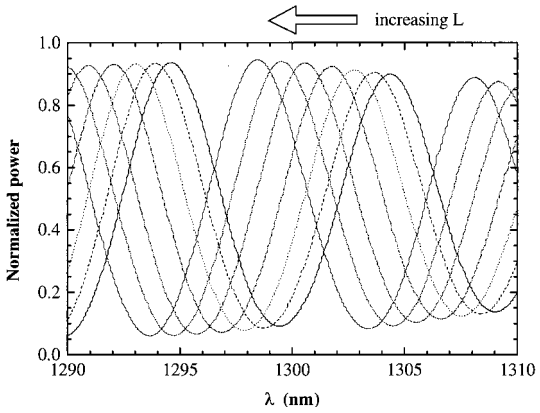

Fig. 4. Typical tuning of the WDM spectral response.

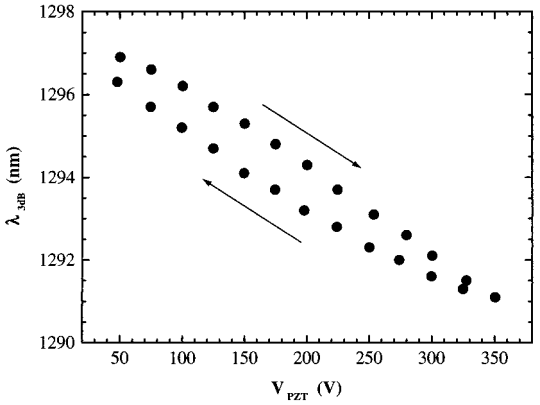

Fig. 6. WDM 3-dB point as a function of applied voltage to the PZT.

use of Eq. (7). That is, for tuning the WDM over the range in which the Bragg wavelength varies (a few nanometers), the elongation of the WDM structure must exceed 15 μm. This elongation was achieved with a PZT bimorph disk translator as shown in the inset of Fig. 3. First-measurement tests demonstrated a nonlinear relation between the integrator output voltage and the Bragg wavelength shift. Also, hysteresis behavior was observed when strain or temperature cycles were applied to the FBG. This is a well-known characteristic of bimorph PZT's. For evaluating the real displacement of the PZT and consequently the WDM elongation, a small mirror was attached to the PZT. The displacement of this mirror was then measured by use of a free-space Michelson interferometer illuminated by a He–Ne laser. The relation between the 3-dB wavelength of the WDM and the applied voltage to the PZT was investigated as shown in Fig. 6. As can be seen, the response is not linear. However, when real WDM elongation was used rather than the PZT voltage (Fig. 7), a good linearity was obtained for the entire cycle, validating the basic principle of the proposed technique. Linear fitting to experimental data indicates that $\Delta\lambda_{3dB}/\Delta L = -0.17$ nm/μm, in good agreement with the theoretical value presented above.

These results indicate that, owing to the PZT hysteresis, neither V_{PZT} nor the integrator signal linearly depends on the change in Bragg wavelength. For the Bragg wavelength shifts to be accurately measured, real elongation of WDM should be monitored. Figure 8 shows the system response when the sensing FBG was subject to a cyclic temperature variation of ≈100 °C. A good linear relation is observable, and from data in this figure a resolution of 0.2 °C/$\sqrt{\text{Hz}}$ can be calculated for temperature measurements. The system response to an applied strain cycle is shown in Fig. 9, and a resolution of 2.1 με/$\sqrt{\text{Hz}}$ can be calculated from data in this figure. Again a good linear relation is observable. As discussed above, closed-loop operation is essential in obtaining linearity over a large measurement range. For a comparative study the system was operated in open loop and strain was applied to the FBG sensor (Fig. 10). As predicted, typical sinusoidal output was observed that limits the linear measurement range to approximately 1 mε.

It must be emphasized that the resolutions obtained were determined not only by the system performance (noise and WDM selectivity) but also by errors associated with measuring the PZT displace-

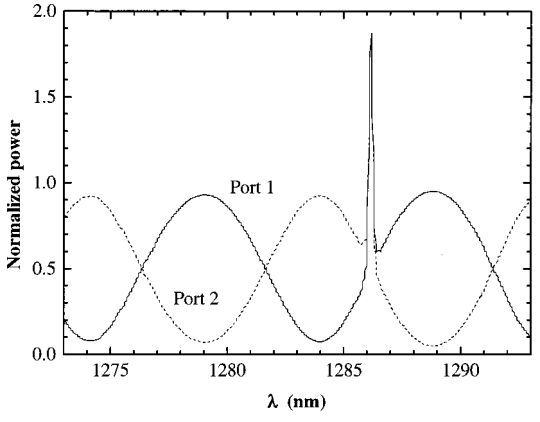

Fig. 5. The 3-dB lock point: reflected spectrum from FBG and WDM transfer function.

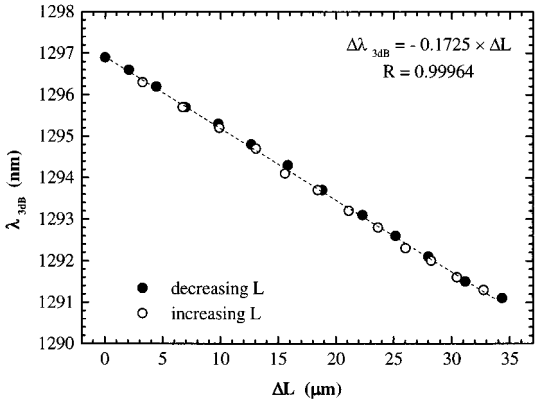

Fig. 7. WDM 3-dB point as a function of PZT displacement.

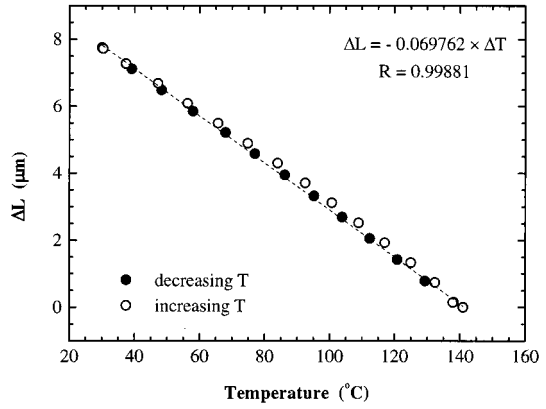

Fig. 8. System response to the applied temperature cycle.

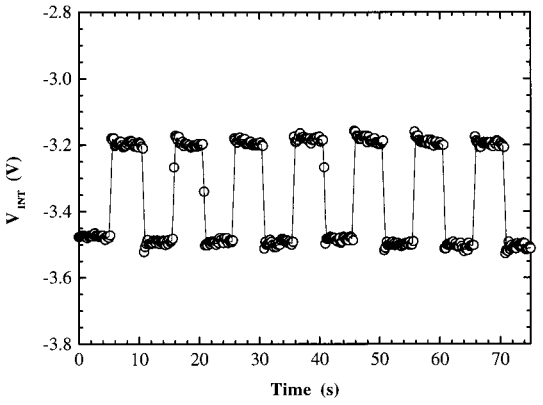

Fig. 11. System response to a strain square wave with 45.3-με amplitude.

ment with a nonoptimized external interferometer. As mentioned above, the free-space interferometer was added to the proposed interrogation scheme only to correct for PZT hysteresis. In fact, if the integrator output was monitored rather than the auxiliary interferometer output, better sensitivity should be expected, although in this case the linearity becomes degraded. This result can be confirmed from data in Fig. 11 where the system response (V_{INT}) to a strain square wave with amplitude of 45.3 με is shown.

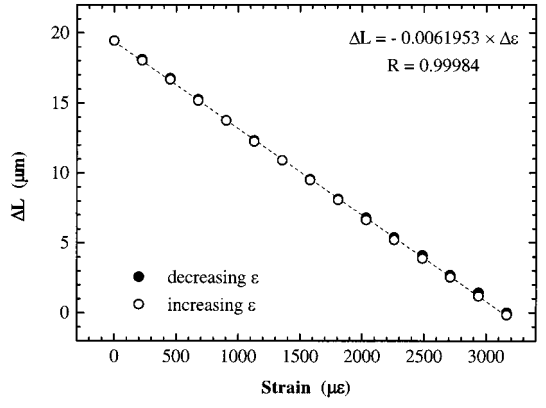

Fig. 9. System response to the applied strain cycle.

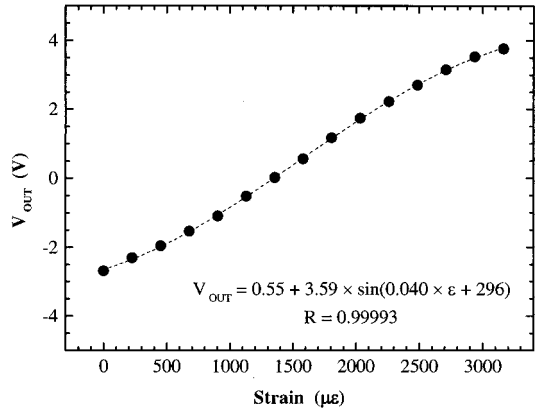

Fig. 10. System response to the applied strain in open-loop operation.

When the observed signal-to-noise ratio is used, a resolution of 0.3 $\mu\varepsilon/\sqrt{\text{Hz}}$ can be calculated. From this value and data in Fig. 9 a dynamic range of 80 dB for strain measurements can be obtained, which is a good indication of the system performance working in an ideal situation.

For evaluating the system response to ac signals, a sinusoidal strain signal with 0.3-με amplitude and 200-Hz frequency was applied to the FBG. Because this frequency is beyond the system bandwidth (≈10 Hz), the output signal must be detected after the differential amplifier (V_{OUT}). Figure 12 indicates a signal-to-noise ratio of 14 dB, resulting in an ac strain sensitivity of 42 $n\varepsilon/\sqrt{\text{Hz}}$.

The maximum wavelength tuning range obtained with the implemented assembly was measured as 15 nm and was limited by the maximum voltage that can be applied to the PZT. This value is sufficient for most FBG sensing applications. However, as mentioned above, the PZT stretcher used in this experiment exhibited a strong hysteresis behavior with the applied voltage. For using the signal applied to the PZT as a direct output of the system and for avoiding measuring the PZT real displacement, a reference technique should be implemented. For ex-

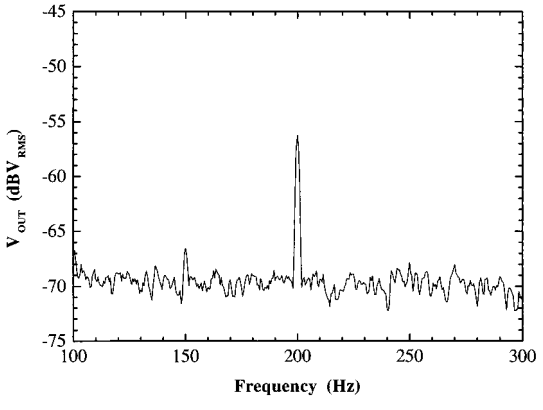

Fig. 12. System response to an ac strain signal with 0.3-με amplitude.

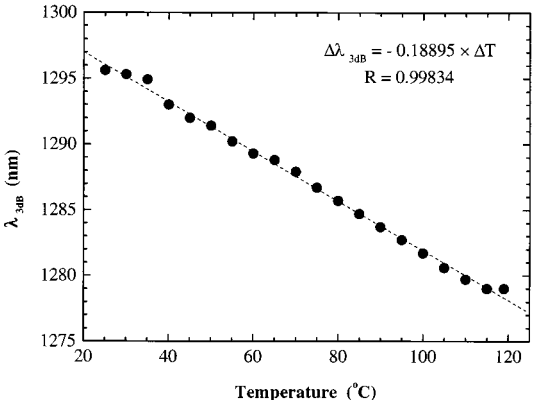

Fig. 13. WDM temperature dependence.

ample, if a small ac signal were applied to the PZT in addition to the compensation signal, an intensity reference would be generated that could be used to locate the operating point on the hysteresis curve and correct for the nonlinearity. An alternative solution would be the use of less efficient PZT stretchers exhibiting low hysteresis. In this case it is possible to design a feedback circuitry that resets itself when the output voltage reaches a certain maximum value. The periodic nature of the WDM device allows a second 3-dB point to be used when the full range of the first operating point has already been utilized.

Finally, we examined the effect of induced additional insertion loss and thermal stability of the WDM used in this experiment. The insertion loss over the range of elongation used in this experiment was found to be constant within an error of 0.1 dB. To examine the temperature dependency of the WDM spectral characteristic curve, we chose a 3-dB point and measured its shift as the temperature was changed by ≈100 °C (Fig. 13). The best linear fit depicts a wavelength-to-temperature dependency factor of −0.18 nm/°C. This degree of sensitivity can be easily handled by proper shielding of the WDM device.

4. Conclusion

We have presented a closed-loop technique for measuring Bragg wavelength shifts based on active wavelength tuning of a biconical WDM. A theoretical model was developed to assist the fabrication of optimized high selective couplers for this purpose. By direct measurement of the WDM elongation in closed-loop operation, resolutions of 0.2 °C/$\sqrt{\text{Hz}}$ and 2.1 $\mu\varepsilon/\sqrt{\text{Hz}}$ were obtained for dc temperature and strain measurements. For ac strain measurements a resolution of 42 $n\varepsilon/\sqrt{\text{Hz}}$ was obtained at 200 Hz.

L. A. Ferreira and F. M. Araújo acknowledge financial support from Programa PRAXIS XXI. F. Farahi acknowledges support from National Science Foundation grant DMI-9413966.

References

1. E. Udd, C. M. Laurence, and D. V. Nelson, "Development of a three-axis strain and temperature fiber optic grating sensor," in *Smart Structures and Materials 1997: Smart Sensing, Processing, and Instrumentation*, R. O. Claus, ed., Proc. SPIE **3042,** 229–236 (1997).
2. R. M. Measures, A. T. Alavie, R. Maaskant, M. Ohn, S. Karr, and S. Huang, "A structurally integrated Bragg grating laser sensing system for a carbon fiber prestressed concrete highway bridge," Smart Mater. Struct. **4,** 20–30 (1995).
3. H. Sing and J. S. Sirkis, "Simultaneously measuring temperature and strain using optical fiber microcavities," J. Lightwave Technol. **15,** 647–653 (1997).
4. K. O. Hill and G. Meltz, "Fiber Bragg grating technology fundamentals and overview," J. Lightwave Technol. **15,** 1263–1276 (1997).
5. A. D. Kersey, M. A. Davis, H. J. Patrick, M. LeBlanc, K. P. Koo, C. G. Askins, M. A. Putnam, and E. J. Friebele, "Fiber grating sensors," J. Lightwave Technol. **15,** 1442–1462 (1997).
6. S. M. Melle, K. Liu, and R. M. Measures, "Practical fiber-optic Bragg grating strain gauge system," Appl. Opt. **32,** 3601–3609 (1993).
7. M. A. Davis and A. D. Kersey, "All-fiber Bragg grating strain-sensor demodulation technique using a wavelength division coupler," Electron. Lett. **30,** 75–77 (1994).
8. Q. Zhang, D. A. Brown, H. Kung, J. E. Townsend, M. Chen, L. J. Reinhart, and T. F. Morse, "Use of highly overcoupled couplers to detect shifts in Bragg wavelength," Electron. Lett. **31,** 480–482 (1995).
9. A. B. Lobo Ribeiro, L. A. Ferreira, M. Tsvetkov, and J. L. Santos, "All-fiber interrogation technique for fiber Bragg sensors using a biconical fiber filter," Electron. Lett. **32,** 382–383 (1996).
10. L. A. Ferreira and J. L. Santos, "Demodulation scheme for fiber Bragg sensors based on source spectral characteristics," Pure Appl. Opt. **5,** 257–261 (1996).
11. A. D. Kersey, M. A. Davis, and T. Tsai, "Fiber optic Bragg grating strain sensor with direct reflectometric interrogation," in *Proceedings of the Eleventh International Conference on Optical Fiber Sensors*, Y. Ohtsuka and T. Yoshino, eds. (Japan Society of Applied Physics, Sapporo, Japan, 1996), pp. 634–637.
12. T. Coroy and R. M. Measures, "Active wavelength demodulation of a Bragg grating fiber optic strain sensor using a quantum well electroabsorption filtering detector," Electron. Lett. **32,** 1811–1812 (1996).
13. A. D. Kersey, T. A. Berkoff, and W. W. Morey, "Multiplexed fiber Bragg grating strain-sensor system with a fiber Fabry–Perot wavelength filter," Opt. Lett. **18,** 1370–1372 (1993).
14. M. G. Xu, H. Geiger, J. L. Archambault, L. Reekie, and J. P. Dakin, "Novel interrogating system for fiber Bragg grating sensors using an acousto-optic tunable filter," Electron. Lett. **29,** 1510–1511 (1993).
15. D. A. Jackson, A. B. Lobo Ribeiro, L. Reekie, and J. L. Archambault, "Simple multiplexing scheme for a fiber-optic grating sensor network," Opt. Lett. **18,** 1192–1194 (1993).
16. M. J. F. Digonnet and H. J. Shaw, "Analysis of a tunable single mode optical fiber coupler," J. Quantum Electron. **QE-18,** 746–754 (1982).
17. H. Berthou and L. Falco, "Switching characteristics of a piezoelectrical actuated evanescent-wave directional coupler," Electron. Lett. **23,** 469–471 (1987).
18. J. Bures, S. Lacroix, and J. Lapierre, "Analyse d'un coupler bidirectionnel à fibre optiques monomodes fusionnées," Appl. Opt. **22,** 1918–1922 (1983).
19. B. S. Kawasaki, M. Kawachi, K. O. Hill, and D. C. Johnson, "A single-mode-fiber coupler with a variable coupling ratio," J. Lightwave Technol. **1,** 176–178 (1983).
20. T. A. Birks, "Twist-induced tuning in tapered fiber couplers," Appl. Opt. **28,** 4226–4233 (1989).
21. S. Celashi, J. T. De Jesus, and F. M. Smolka, "All-fiber tunable beam splitter," in *Conference on Lasers and Electro-Optics*,

Vol. 7 of 1988 Technical Digest Series (Optical Society of America, Washington, D.C., 1988), pp. 358–359.
22. A. Booysen, S. J. Spammer, and P. L. Swart, "Ratiometric fiber optic sensor utilizing a fused biconically tapered coupler," in *Fiber Optic and Laser Sensors IX*, R. P. DePaula and E. Udd, eds., Proc. SPIE **1584,** 273–279 (1991).
23. R. G. Lamont, D. C. Johnson, and K. O. Hill, "Power transfer in fused biconical-taper single-mode fiber couplers: dependence on external refractive index," Appl. Opt. **24,** 327–332 (1995).
24. M. B. J. Diemeer, W. J. De Vries, and K. W. Benoist, "Fused coupler switch using a thermo-optic cladding," Electron. Lett. **24,** 457–458 (1988).
25. F. P. Paine, C. D. Hussey, and M. S. Yataki, "Modeling fused single-mode-fiber couplers," Electron. Lett. **21,** 461–462 (1985).
26. R. P. Kenny, T. A. Birks, and K. P. Oakley, "Control of optical fiber taper shape," Electron. Lett. **27,** 1654–1656 (1991).
27. J. D. Love and W. M. Henry, "Quantifying loss minimization in single-mode fiber tapers," Electron. Lett. **22,** 912–914 (1986).